Proceedings of the 6th International Conference on Energy Harvesting, Storage, and Transfer (EHST'22)
Niagara Falls, Canada – June 08-10, 2022
Paper No. 133
DOI: 10.11159/ehst22.133

The Design of a Savonius Wind Turbine with Guide Vanes - A Computational Approach

Wimukthi Senarathna[1], Madhawa Fernando[1], Tharindu Silva[1], Chamil Abeykoon[2]
[1]University of Moratuwa, Bandaranayake Mawatha, Moratuwa 10400, Colombo, Sri Lanka
Emails: wimukthis@uom.lk, nimeshm@uom.lk, Tharindu1997.silva@gmail.com
[2]Department of Materials, Faculty of Science and Engineering, The University of Manchester, Oxford Road, M13 9PL, Manchester, UK, *Email: chamil.abeykoon@manchester.ac.uk*

Abstract **-** In this study, a Savonius vertical axis wind turbine (SVAWT) has been developed with omnidirectional guide vanes to increase the performance of the wind turbine. SVAWT is a promising wind turbine for stand-alone power generation to cater the energy demand in rural settings. However, Savonius rotors typically possess low wind energy extraction characteristics compared with other wind turbine types. Therefore, this study is focused to design and develop an SVAWT using more suitable/optimized blade configurations and compatible omnidirectional guide vanes to enhance their power performance characteristics. First, a modelling framework was developed based on a numerical approach to predict the performance of an SVAWT. Then the proposed design framework was validated using the data reported in the literature to identify the performance and key characteristics parameters of SVAWT through research data, to develop a semi-empirical relation for the performance evaluation of the wind turbine, and to evaluate the effect of integrating omnidirectional guide vanes to SVAWT. The results demonstrate that up to 80% gain of average power could be achieved at TSR = 0.8 with the integration of the proposed blade configuration with guide vanes.

Keywords**:** Savonius vertical axis wind turbine, Power Coefficient, Renewable Energy, Guide vanes, CFD modelling

1. Introduction

Non-renewable energy resources have been used to fulfil the majority of global energy needs over the last few decades. With the indiscriminate exploitation and predicted depletion of fossil fuels, consequences such as environmental pollution, the greenhouse effect, and climate change have become major global concerns in the present time. Therefore, the development of renewable energy sources under sustainable energy criteria has received wide attention among researchers and authorities worldwide [1]. When considering the recent status of the global renewable energy sector, the wind and solar PV sectors have rebounded over 2020 by increasing the global installed renewable energy capacity by 10% of the existing capacity of 2839 GW [2]. Obviously, the whole world is moving towards green/renewable sources while the majority of the countries have been pledged to achieve NET ZERO by 2050 [2]. Among renewable energy sources, wind energy is one of the sources which has been used for thousands of years (in different forms) and also one of the potential sources of current global renewable energy plans. As per known records, wind power has been utilized by Mesopotamians for irrigation activities since 1700 B.C. Similarly, Afghanistan and Iran have used windmills in 700 A.D [3], half-covered flow augmentation has been used in vertical axis Persian windmills [3] and Sri Lanka had ancient wind driven iron smelting furnaces since the third century B.C.[4].

Horizontal axis wind turbines and vertical axis wind turbines (VAWT) are the main two types of wind turbines. VAWTs are mainly categorized as Darrius and Savonius wind turbines. The Savonius wind turbine is a type of VAWT, which was invented by S.J. Savonius in 1925 [5]. It was reported that the maximum efficiency for the conventional Savonius turbine is less than 25% [6], although some experimental designs might reach of up to 35% [7]. Such a low efficiency is mainly due to some factors such as working at low tip speed ratios, low power coefficient of the rotor, issues in structural features, and also these are normally installed at relatively shorter towers and hence they may not be exposed to strong wind forces at higher heights. However, the grid electricity demand of rural and urban environments may be reduced using the Savonius wind turbine as an alternative energy source as it is a promising design for stand-alone power generation [8]. Moreover, as was mentioned above, Savonius rotors possess low wind energy extraction characteristics and hence further improvements to their design should be invaluable. According to the literature, the power coefficient of a SVAWTs without a stator lies in

the range of 0.10 - 0.30 [8]. Despite SVAWTs' reported low power performance, there are some favourable design considerations such as design simplicity, omnidirectional operation, ease of installation, the ability for self-starting, less proneness to wear, ease of manufacture, less noise, the option for various blade configurations, good starting torque characteristics, etc. associated with them [1],[6],[10].

Considerable amount of researches have been reported in the last few decades to improve the performance of the SVAWT considering various factors such as the number of blades, blade configurations (semi-circular, twisted, helical, etc.), characteristic parameters of blades, number of stages, stators, etc. [1],[6]. A Guide vane is a stator design that is introduced to optimise a wind turbine performance [9]. Work by Al-Ghriybah and others [11] demonstrated that the use of stators to reduce negative torque on the rotor and to increase the upstream wind velocity can enhance the performance of the SVAWTs [11]. The performance of a SVAWT can be greatly increased with carefully designed blade configurations together with compatible omnidirectional guide vanes (ODGV) [1],[8],[13] see Figure 1. Therefore, this study focuses on the design and development of a Savonius VAWT using a selected high-performance blade configuration and compatible omnidirectional guide vanes.

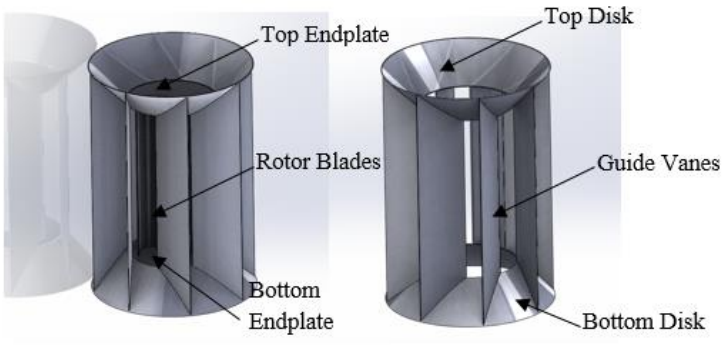

Figure 1 Nozzle- ODGV Combination

2. Methodology

2.1. Selection of performance and characteristic parameters

Due to the unavailability of a proper analytical model to estimate the flow field around the SVAWT, the performance of SVAWT is usually estimated by approaches such as wind tunnel testing, field experiments, and Computational Fluid Dynamics (CFD) simulation methods [1]. Also, the performance of SVAWT is usually represented in terms of the parameters such as the power coefficient (C_p), tip speed ratio (TSR), and dynamic torque coefficient (C_T), and the related equations are presented by (1), (2) and (3), respectively. Where $P_{Turbine}$ is the power produced by the wind turbine, $P_{Available}$ is the power available to be extracted from the wind, T is the dynamic torque of the wind turbine, ω is the rotational speed of the rotor, ρ is the density of air, A is the swept area of the rotor V is the free stream velocity, λ is the tip speed ratio, R is the rotor radius [6]. The power coefficient (C_p) represents the fraction of the power extracted from the available power of undisturbed incoming airflow [6], and can be presented by Eq. (4) as well.

$$C_P = \frac{P_{Turbine}}{P_{Available}} = \frac{T\omega}{0.5\rho AV^3} \quad (1)$$

$$\lambda = TSR = \frac{R\omega}{V} \quad (2)$$

$$C_T = \frac{T}{0.5\rho AV^2R} \quad (3)$$

$$C_P = \frac{P_{Turbine}}{P_{Available}} = \frac{T\omega}{0.5\rho AV^3} = \frac{T}{0.5\rho AV^2R} \times \frac{R\omega}{V} = C_T \times TSR \quad (4)$$

The bucket overlap ratio, bucket spacing, the number of blades, rotor stages, end plates, aspect ratio, blade configurations, Reynolds number, turbulent scales, and stators are among the main characteristic parameters that should be appropriately considered when developing an SVAWT [1], [13], [14].

2.1.1. Effect of spacing and overlap ratio

Blade spacing is the distance between the two blades as shown in Figure 2. The null spacing gives the best performance for semi-circular Savonius blade profiles because the air does not properly focus on the concave side of the returning blade. However, most of the high-performance rotors have carefully selected non-zero bucket spacing [1], [7]. The overlap ratio is the ratio between the overlap distances to the rotor diameter. The non-zero overlap ratio reduces the wake region from the blockage effect and increases the flow rate. There is no consensus about an optimal overlap ratio, and it should be determined to match with other parameters.

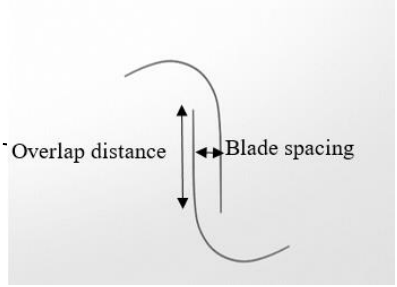

Figure 2: Overlap distance and blade spacing

2.1.2. Effect of endplates and effect of aspect ratio (H/D)

The endplates are the circular plates that are located at the top and bottom of the rotor as shown in Figure 1. It maintains a suitable pressure difference between concave and convex blades by preventing the escape of air from the concave buckets to the air stream. It has been suggested that a Savonius rotor with an endplate diameter equal to 1.1 times the rotor diameter gives the highest performance. [1], [15]. Aspect ratio (*AR*) is the ratio between the turbine height (*H*) and the rotor diameter (*D*), and hence it is related to the inertia, momentum, and acceleration of the rotor. Increasing the aspect ratio advances the performance of the rotor and most studies have reported considerably good results for aspect ratios of about 2 [1].

2.1.3. Effect of the number of blades, stages, and blade configuration

The addition of blades increases the oscillating torque and also reduces the maximum moment and power coefficients along the rotation as the bucket deflects the airflow that focuses on the next advancing blade. According to the literature, two-bladed Savonius rotors give the best performance concerning the number of blades [13]. An increase in the number of stages gives a uniform torque. When the first stage generates a positive torque, the second stage generates a negative torque which causes an overall reduction of the power coefficient, this can be considered as one of the main disadvantages of multi-staged rotors. Therefore, it has been concluded that the single-stage rotors can provide the best performance [1], [13], [15].

Table 1: Summary of some of the previously reported blade performance

Author(s)	**Blade Configuration**	**Testing Method**			
		Experimental		**CFD**	
		C_p	*TSR*	C_p	*TSR*
Roy and Saha [6]	**Newly developed (configuration-(a))**	**0.31**	**0.82**		
	Modified batch	0.30	0.80		
	Benesh	0.29	0.80		
	Semi elliptic	0.26	0.75		
	Conventional	0.23	0.73		
Alom and Saha [7]	**Elliptical (Configuration-(b))**	**0.19**	**0.78**	**0.340**	**0.80**
	Modified batch	0.162	0.80	0.304	0.80
	Benesh	0.159	0.60	0.294	0.80
	Semi-circular	0.158	0.78	0.272	0.80
Mohamed and others [12]	**Optimum blade configuration(2D) (configuration-(c))**			**0.298**	**0.70**

After studying plenty of literatures, the configurations presented in Table 1, a newly developed blade by Roy and Saha [6], an elliptical blade [7], and the optimal blade configuration reported by Mohamed and others [12] were selected as the best blade configurations for the design of SVAWT in this study. The details of the selected blade configurations are shown in Figure 3.

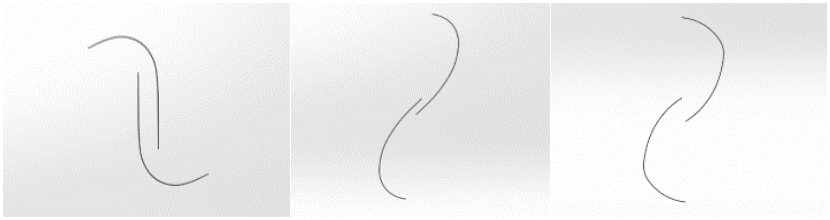

Figure 3: Configuration – (a) [6], Configuration – (b) [7], Configuration – (c) [12]

2.2. Development of the semi-empirical relation for the performance evaluation of a SVAWT

The importance of experiments arises with the validation of simulation results and when further modifying the design proposed numerically. A SVAWT's wind rotor can be designed with and without guide vanes. Dimensional analysis has been performed to get the reduced version of the equation as shown in EQ. (5) by utilizing logical reasoning:

$$C_p = f(TSR) \tag{5}$$

According to equations (2) and (5), the rotational speed (ω) can be varied by changing the load on the rotor. From that, different *TSR* values can be obtained from the experiment to formulate a *TSR* vs C_p plot. If the dependence of the Reynolds number on C_p is to be evaluated, different free stream velocities can be used for each *Re* number. Therefore, a set of curves can be plotted for different velocities or *Re* numbers. But this study, the effect from the Reynolds number was neglected as it is in the order of 1×10^5.

2.3. Integrating the SVAWT with Power Augmentation Devices

Power Augmentation devices can be categorized mainly into Nozzles, Guide vanes, Windshields, Curtain Plates, and Deflector plates [11]. Considering the typical high performance of nozzle type, the omni directionality of the guide vanes and their practically proven performance, both nozzle geometries, and guide vane geometries can be combined to generate a power augmentation device that can increase the power coefficient. A guide vane angle of 60 degrees to the flow direction (see Figure 4) and 4 pairs of guide vanes have performed better and the results have also been validated using the experimental setups in the literature [16], [17].

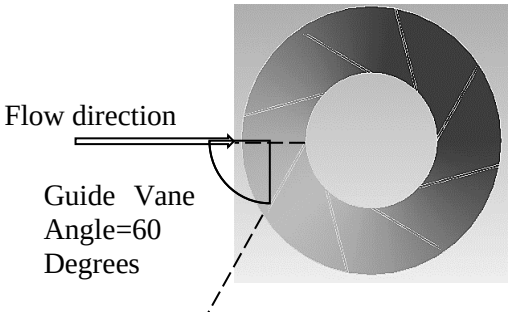

Figure 4: Guide vane arrangement

2.4. Development of the CFD modelling framework for a SVAWT

The validation of the CFD simulation is done using a commercial software package, ANSYS FLUENT 19 R3, and the configuration-(a) blade design by Roy and Saha [6] is used to validate the CFD modelling framework. The reason for the utilization of the configuration-(a) is the availability of experimental results. Three different categories of fluid-solid coupling were identified from the previous works of O'Brien and others [18] and Friedrich and others [19]. Atmospheric air at 15° Celsius at the sea level conditions and Re number of 1×10^5 were used in the validation of the CFD modelling framework. Following the reference results, the simulations were conducted for the TSR below 1.

Three governing equations from the conservation of mass and momentum are formulated in the solver setup while neglecting the third dimension and the energy equation due to the negligence of the effect from temperature. The fixed tip speed ratio technique is used for the simulations since it gives accurate results while in transient conditions, consuming less

computational power compared with other available methods [20]–[24]. Therefore, the fluid-solid coupling technique used in this study is the one-way solid to fluid reaction coupling technique. The rotational motion of the rotor was provided by a constant azimuthal angle increment per time step of the rotating domain. This kind of analysis evaluates the effect of fluid flow, while the rotor is being rotated at a constant pre-determined speed [21],[22],[23]. The discretized governing equations are solved for each cell in the mesh by the finite volume method. The $k-\omega$ SST (Shear Stress Transport) turbulence model was selected as it suggests for separating flows and compressible flows under adverse pressure gradients while producing reliable results as described in the literature [25]. The coupled solution algorithm was used following the pressure-based approach since it can be utilized with large time steps, unstructured mesh providing the benefits of robustness and convergence [25]. For the Gradient, the least squire cell-based approach was used considering the unstructured mesh. The y^+ value below 1 was maintained to be compatible with the turbulence model and to keep the simulation stability, the Courant number close to 1 was maintained [25]. In the solver setup, the 2nd order implicit and upwind schemes were used respectively for the time differencing and spatial discretization of governing equations.

Different factors were affected when validating the computational framework using the existing experimental data. Since the blades are not helical and have the same horizontal cross-section throughout the horizontal plane and due to the high computational cost of 3D geometry, 2D simulations are carried out. Therefore, there could be some deviation between the experimental and computational results due to the negligence of the 3D effect. The selected rotor has two blades and two endplates, but endplates were neglected in the 2D simulations because only the cross-section of the rotor at the centre is considered. As stated in 2.1.2, the endplates enhance the performance of the turbine [1] and hence the CFD results are also affected by this factor.

The geometry of the simulation was modified after the addition of the stator as shown in Figure 5. The guide vane has a diameter of twice the rotor with a sheet thickness of 1.5 mm. It also maintains an angle of 60 degrees to the flow direction. The same ANSYS Fluent software package was used to implement/analyse the model. For comparison, two simulations were carried out, one with the stator and another without the stator with newly generated mesh, maintaining the same mesh control settings.

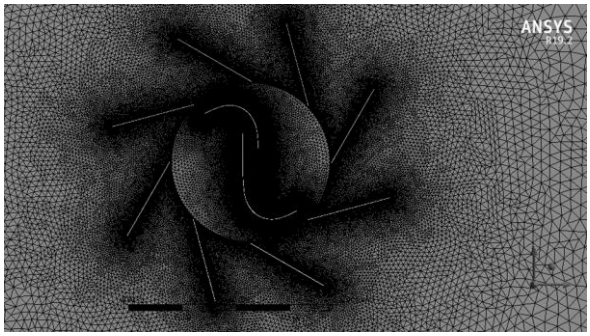

Figure 5: Rotor with guide vane mesh

3. Results And Discussion

3.1. Mesh convergence and Power coefficient (C_p)

The mesh convergence results show a converging behaviour from 1 to 0.75 as shown in Figure 6. Thus, considering the computational limitations the mesh factor of 1 has been selected for simulations of this study. Instantaneous C_m values that have been obtained for each time step (see Figure 7) were averaged to get the global C_m value. Using the average C_m values that have been calculated using only the steady-state C_m values were used to calculate the C_p using Eq. (4) and related values are presented in Table 2.

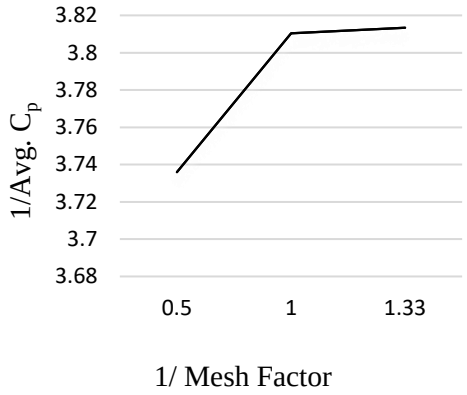

Figure 6: Mesh convergence plot

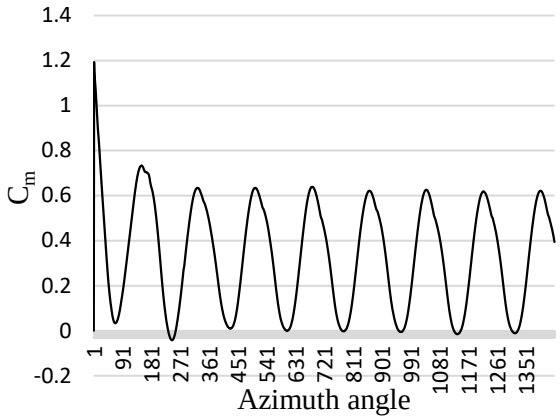

Figure 7: Azimuth angle vs C_m

Table 2: Deviation in power coefficient

Rotational Cycle	**C_p at TSR=0.82**	**Deviation (%)**
2nd Cycle	0.2922	-
3rd Cycle	0.2676	8.43
4th Cycle	0.2573	3.82
5th Cycle	0.2502	2.78

The C_p value was converged to 0.2502 at *TSR* of 0.8 at the 5th rotational cycle. Similarly, for other *TSR* values, the results have been plotted against each other. C_p vs *TSR* plot reaches a maximum of 0.2502 at around the TSR value of 0.8 for both numerical and experimental conditions as shown in Figure 8. Then the numerical results of this study were compared with the experimental results reported by Roy and Saha [6] as illustrated in Table 3. The results show a similar trend when compensating with previously mentioned deviations available in the present study.

Table 3: A comparison of the CFD results of the present study and with experimental results of Saha [6]

TSR	**Numerical C_p**	**Experimental C_p**	**Deviation %**
0.2	0.0883	0.09	1.78
0.6	0.2072	0.29	28.52
0.82	0.2501	0.31	19.30
1	0.2120	0.275	22.89

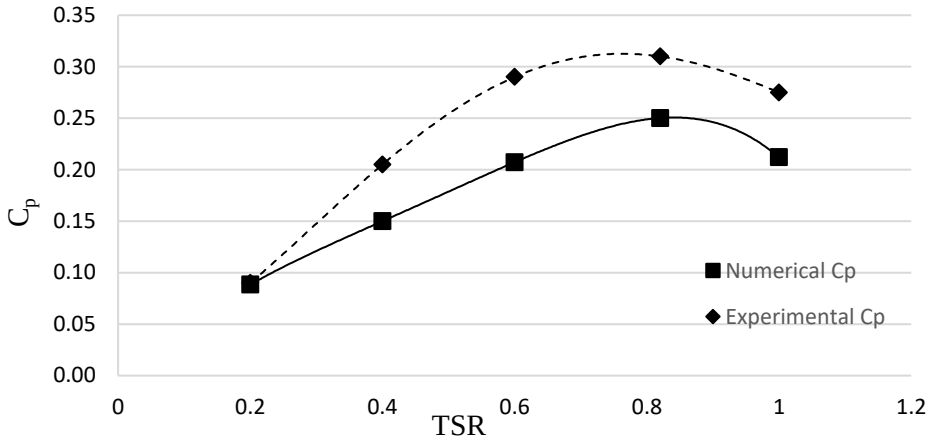

Figure 8: Results Comparison

As shown in Table 3, the maximum deviation between the numerical and experimental results was 28.5% at *TSR* =0.6. In this study, a minimum reduction of 25% in C_p was expected in the CFD results due to the negligence of the effect of endplates. Therefore, the results obtained are in the expected range and it could be claimed that the proposed CFD modelling framework provides reasonably accurate results for the simulation of the Savonius rotor. Using the same computational model to evaluate three reported blades in the literature, the results presented in Table 4 were obtained from simulations for the same flow parameters.

Table 4: C_p value comparison for three-blade configurations

Rotational Cycle	**Configuration-(a)** [6] $\mathbf{C_p}$	**Configuration-(b)** [7] $\mathbf{C_p}$	**Configuration-(c)** [12] $\mathbf{C_p}$
2nd	0.2771	0.2735	0.2847
3rd	0.2661	0.2585	0.2597
4th	0.2573	0.2497	0.2505

All three blade configurations showed quite identical results. Therefore, the selection of the blade configuration was performed considering the ease of fabrication. The newly developed blade by Roy and Saha [6] has the least complex shape, and hence it was selected as the best blade configuration for the design of SVAWT by considering the C_p and the relative ease of fabrication.

3.2. The guide vane simulation results

Figure 9 shows moment coefficient variation with the azimuth angle for numbers of the rotational cycle until it reaches the acceptable convergence level. The rotor results converged to less than 5% at the 4th cycle and the rotor with the stator showed cyclic variations due to variation of the dynamic torque. When getting the C_m values from the chart, the diameter of the rotor is used as the swept area in the reference table of the ANSYS setup in both cases. From Eq. (4), it can be seen that the C_p of the whole turbine is reduced after the integration of the guide vanes to the rotor. The positive torque is generated for almost full rotation at TSR = 0.8 at the convergence phase for both cases except very small range azimuthal angles for the turbine with ODGV case. The turbine without ODGV generates 2.41 W of power at 0.8. The turbine with ODGV generates 4.34 W of power at TSR = 0.8 as the outer diameter of the stator is 2*D* and the height of the stator is 2.9*D* due to 45 degrees nozzle angle. Therefore, the swept area of the SVAWT with a stator is 0.23 m^2. Due to the increase of the swept area of the turbine by 187.5%, the power generated has been increased by 80%.

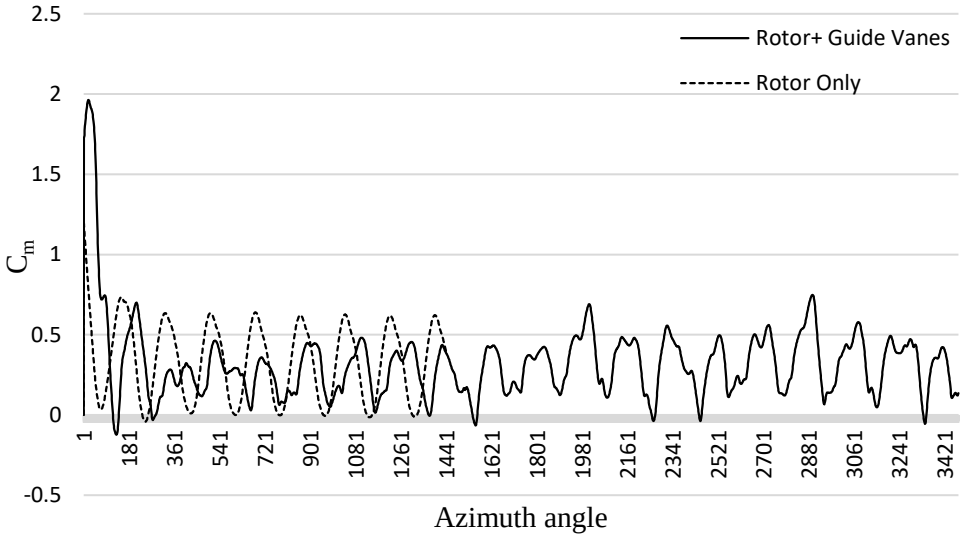

Figure 9: Comparison of the guide vane results

4. Conclusions

This study proposes a Savonius VAWT with a more suitable blade configuration integrated with compatible omnidirectional guide vanes to improve the power extraction performance. The performance of the Savonius VAWT has increased by the reduction of the negative torque portions by changing and regulating the flow direction, increasing the wind speed at the wind rotor. Also, a rotor that has the same size as the ODGV without guide vanes will produce more power than the rotor with guide vanes while reducing the manufacturing cost. However, when the rotor diameter is increased, the inertia of the rotor will increase due to the rotating mass. Therefore, considering the advantages of omnidirectional guide vanes such as capturing wind from all directions and their ability to direct towards blades, protecting birds or objects from collisions, and minimizing the possible damages to the blades, make the ODGV a viable option for wind turbines in the rural context. Since the blade configuration was selected based on the highest power performances and the ease of fabrication, the integrated SVAWT is suitable to be installed in rural areas where the relevant wind resources are available.

All three blades showed C_p values in the range of 0.25 – 0.26 with the proposed model. Therefore, by considering the power coefficient and the ease of manufacturing, the blade proposed by Roy and Saha [6] was selected as the blade configuration for this study. The final simulation shows the significant enhancement of the power performance of the rotor with the integration of the ODGV. At the considered operating conditions, an 80% increment of the turbine power production was observed due to the 187% increment of the swept area of the rotor with ODGV. Also, the negative torque region has reduced almost completely to the positive region for the full rotation of the rotor.

The present study proves the ability of the integrated rotor to generate more power due to the best-selected blade configuration and the ODGV than the rotor without ODGV. The proposed version of the turbine will be a significant solution to the energy shortages of rural areas. The proposed numerical model of SVAWT can be further improved by various blade and guide vane modifications. Furthermore, more simulations and experimental analysis are required to study the rotor with guide vanes to broaden the understanding of the effects of different parameters. Blade modifications (such as blade ducts, aerofoil shape blades, and blade shape optimization) and guide vane modifications (such as the variable guide vanes and guide vane shape optimization) can be studied further. Finally, an analytical method can be developed to calculate the power coefficient of a SVAWT from the experimental results.

5. References

[1] J. V. Akwa, H. A. Vielmo, and A. P. Petry, "A review on the performance of Savonius wind turbines," *Renew. Sustain. Energy Rev.*, vol. 16, no. 5, pp. 3054–3064, 2012, doi: 10.1016/j.rser.2012.02.056.

[2] R. E. N. Members, *Renewables 2021 global status report*. 2021.

[3] R. G. J. Twele, *Wind Power Plants: Fundamentals, Design, Construction and Operation*. 1967.

[4] A. A. K. Kumbalathara, D. D. Liyanage, S. Witharana, J. K. A. T. Rajika, M. Narayana, and K. C. N. Fernando, "Simulation of ancient wind-driven iron smelting furnaces of Sri Lanka," *MERCon 2015 - Moratuwa Eng. Res. Conf.*, pp. 12–17, 2015, doi: 10.1109/MERCon.2015.7112312.

[5] R. Kumar, K. Raahemifar, and A. S. Fung, "A critical review of vertical axis wind turbines for urban applications," *Renew. Sustain. Energy Rev.*, vol. 89, no. September 2016, pp. 281–291, 2018, doi: 10.1016/j.rser.2018.03.033.

[6] S. Roy and U. K. Saha, "Wind tunnel experiments of a newly developed two-bladed Savonius-style wind turbine," *Appl. Energy*, vol. 137, pp. 117–125, 2015, doi: 10.1016/j.apenergy.2014.10.022.

[7] N. Alom and U. K. Saha, "Influence of blade profiles on Savonius rotor performance: Numerical simulation and experimental validation," *Energy Convers. Manag.*, vol. 186, no. October 2018, pp. 267–277, 2019, doi: 10.1016/j.enconman.2019.02.058.

[8] D. D. D. P. Tjahjana and others, "Study on performance improvement of the Savonius wind turbine for Urban Power System with Omni-Directional Guide Vane (ODGV)," *J. Adv. Res. Fluid Mech. Therm. Sci.*, vol. 55, no. 1, pp. 126–135, 2019.

[9] E. S. . A. MOHAMED, "A STUDY OF THE INFLUENCE OF GUIDE VANE DESIGN ON SAVONIUS WIND TURBINE PERFORMANCE Thesis," 2015.

[10] W. Tian, B. Song, J. H. Van Zwieten, and P. Pyakurel, "Computational fluid dynamics prediction of a modified savonius wind turbine with novel blade shapes," *Energies*, vol. 8, no. 8, pp. 7915–7929, 2015, doi: 10.3390/en8087915.

[11] M. Al-ghriybah, M. F. Zulkafli, D. H. Didane, and S. Mohd, "Review of the Recent Power Augmentation Techniques for the Savonius Wind Turbines," *J. Adv. Res. Fluid Mech. Therm. Sci. 60*, vol. 1, no. 1, pp. 71–84, 2019.

[12] M. H. Mohamed, G. Janiga, E. Pap, and D. Thévenin, "Optimal blade shape of a modified Savonius turbine using an obstacle shielding the returning blade," *Energy Convers. Manag.*, vol. 52, no. 1, pp. 236–242, 2011, doi: 10.1016/j.enconman.2010.06.070.

[13] H. H. Al-Kayiem, B. A. Bhayo, and M. Assadi, "Comparative critique on the design parameters and their effect on the performance of S-rotors," *Renew. Energy*, vol. 99, pp. 1306–1317, 2016, doi: 10.1016/j.renene.2016.07.015.

[14] B. D. Altan and M. Atilgan, "An experimental and numerical study on the improvement of the performance of Savonius wind rotor," *Energy Convers. Manag.*, vol. 49, no. 12, pp. 3425–3432, 2008, doi: 10.1016/j.enconman.2008.08.021.

[15] U. K. Saha, S. Thotla, and D. Maity, "Optimum design configuration of Savonius rotor through wind tunnel experiments," *J. Wind Eng. Ind. Aerodyn.*, vol. 96, no. 8–9, pp. 1359–1375, 2008, doi: 10.1016/j.jweia.2008.03.005.

[16] A. H. Elbatran, Y. M. Ahmed, and A. S. Shehata, "Performance study of ducted nozzle Savonius water turbine, comparison with conventional Savonius turbine," *Energy*, vol. 134, pp. 566–584, 2017, doi: 10.1016/j.energy.2017.06.041.

[17] M. Mohammadi, R. Mohammadi, A. Ramadan, and M. H. Mohamed, "Numerical investigation of performance refinement of a drag wind rotor using flow augmentation and momentum exchange optimization," *Energy*, vol. 158, pp. 592–606, 2018, doi: 10.1016/j.energy.2018.06.072.

[18] J. F. O'Brien, V. B. Zordan, and J. K. Hodgins, "Combining active and passive simulations for secondary motion," *IEEE Comput. Graph. Appl.*, vol. 20, no. 4, pp. 86–96, 2000, doi: 10.1109/38.851756.

[19] F. K. Benra, H. J. Dohmen, J. Pei, S. Schuster, and B. Wan, "A comparison of one-way and two-way coupling methods for numerical analysis of fluid-structure interactions," *J. Appl. Math.*, vol. 2011, 2011, doi: 10.1155/2011/853560.

[20] N. Alom and U. K. Saha, "Four Decades of Research into the Augmentation Techniques of Savonius Wind Turbine Rotor," *J. Energy Resour. Technol. Trans. ASME*, vol. 140, no. 5, pp. 1–14, 2018, doi: 10.1115/1.4038785.

[21] J. B. S. Kalluvila and B. Sreejith, "Numerical and experimental study on a modified Savonius rotor with guide blades,"

Int. J. Green Energy, vol. 15, no. 12, pp. 744–757, 2018, doi: 10.1080/15435075.2018.1529574.
[22] F. Balduzzi, A. Bianchini, R. Maleci, G. Ferrara, and L. Ferrari, "Critical issues in the CFD simulation of Darrieus wind turbines," *Renew. Energy*, vol. 85, pp. 419–435, 2016, doi: 10.1016/j.renene.2015.06.048.
[23] T. Zhou and D. Rempfer, "Numerical study of detailed flow field and performance of Savonius wind turbines," *Renew. Energy*, vol. 51, no. March 2013, pp. 373–381, 2013, doi: 10.1016/j.renene.2012.09.046.
[24] A. Grönman, J. Backman, M. Hansen-Haug, M. Laaksonen, M. Alkki, and P. Aura, "Experimental and numerical analysis of vaned wind turbine performance and flow phenomena," *Energy*, vol. 159, pp. 827–841, 2018, doi: 10.1016/j.energy.2018.06.204.
[25] *ANSYS Fluent Theory Guide*, vol. 15317, no. November. ANSYS Inc., 2013.